Integrated Synthesis of Nitrogen-Doped Mesoporous Carbon from Melamine Resins with Superior Performance in Supercapacitors

ARTICLE *in* THE JOURNAL OF PHYSICAL CHEMISTRY C · JANUARY 2014

Impact Factor: 4.77 · DOI: 10.1021/jp410198r

2 AUTHORS, INCLUDING:

Meng Li
National University of Singapore
8 PUBLICATIONS **153** CITATIONS

SEE PROFILE

THE JOURNAL OF PHYSICAL CHEMISTRY C

Article

pubs.acs.org/JPCC

Integrated Synthesis of Nitrogen-Doped Mesoporous Carbon from Melamine Resins with Superior Performance in Supercapacitors

Meng Li and Junmin Xue*

Department of Materials Science and Engineering, National University of Singapore, Singapore 117573

Supporting Information

ABSTRACT: An integrated and reproducible chemical process was developed to fabricate the N-doped mesoporous carbon by using melamine resin as nitrogen source. A two-dimensional carbon framework of graphene sheets was also used as a conductive substrate in order to boost the performance of such nitrogen-doped carbon materials. Compared with the pure mesoporous carbon, the as-made nitrogen-doped carbon/graphene electrode materials exhibited suitable pore size distribution, ordered meso-structure, and uniformly dispersed N atoms with tunable doping amount. These unique properties make them promising electrodes for supercapacitors with superior performance. In particular, N-doped carbon and decorated graphene electrodes could deliver the specific capacitance of 238 and 289 F/g at the current density of 0.2 A/g in a three-electrode system. The results from symmetrical two-electrode revealed that the highly N-doped carbon electrodes offered excellent rate capability (ca. 78% retention as the current density increased from 0.1 to 20 A/g) and superior cycling performance (ca. 91% retention after 1000 cycles).

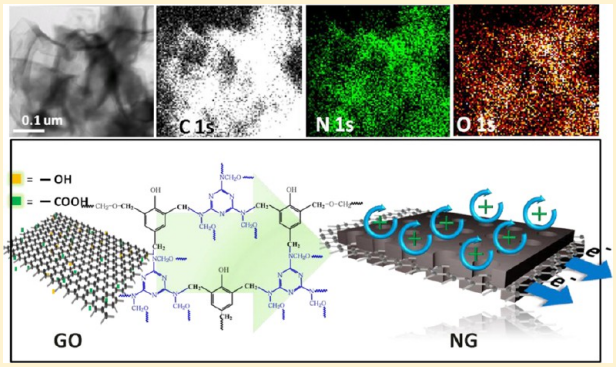

1. INTRODUCTION

To address the increasingly serious environmental problems and excessive consumption of fossil fuels, there has been great urgency in exploiting and refining clean energy technologies as well as more efficient energy storage devices. As one of such energy storage devices, supercapacitors have been widely studied around the world in recent years because they can offer energy density orders of magnitude higher than conventional capacitors, larger power density, and better cycling stability than batteries. The commercially available supercapacitors are mainly electrochemical double-layer capacitors (EDLCs), which store energy through the adsorption of both anions and cations at the interface between electrode and electrolyte.[1,2] Electrode materials are usually considered to play the most important role in the supercapacitors. Among various electrode materials, porous carbon materials have occupied a special place in development of EDLCs due to their high surface area and moderate cost.[3−6] In order to enhance the property of carbonaceous electrode, much attention has been paid to developing the structural design of porous carbon from pore adjusting to morphology transformation. As a result, one-dimensional (1D), two-dimensional (2D), and three-dimensional (3D) structures of carbonaceous materials were developed one after another in recent years. For example, templated carbon, a 3D form of carbon atoms with hierarchical porous channels, has been considered as one of the most promising electrode materials to realize high-energy EDLCs in the past decades.[7−9] Besides the structural design, another way to improve the capacitance is to introduce the pseudocapacitance, such as transition metal oxide and heteroatoms. Transition metal oxides associated with carbonaceous electrodes normally suffer from poor rate capacity and short cycle life because of their poor conductivity and instability. Comparatively, introducing heteroatoms (e.g., N, O, P, B, etc.), especially nitrogen, will improve the carbonaceous electrode performance while maintaining the excellent intrinsic characteristics of carbonaceous materials. Post-treatment method is the primary pathway to introduce heteroatoms into carbon materials. In this method, preformed carbonaceous materials such as activated carbons,[10] carbon nanotubes, templated carbons,[11] and graphenes[12] are treated with N-containing chemicals such as ammonia or urea to attach N atoms. For instance, nitrogen-doped graphene (NG) was fabricated by Li et al. through annealing treatment of graphene oxide (GO) in the atmosphere of ammonia, and the resulting NG exhibited some unique properties including improved conductivity and enhanced capacitance value.[13] However, it is difficult to prepare stable NG with uniform dispersion and tunable N-doping amount by using this method.[14] In order to get more uniform distribution of the heteroatoms in carbon, an in situ synthesis method has been developed, of which N-containing polymeric materials such as poly(acrylonitrile),[15,16] polyaniline,[17,18] pyrrole,[19−22] melamine,[23,24] or N-containing ionic liquids[25] are employed as precursors. For example, Ma et

Received: October 14, 2013
Revised: January 15, 2014
Published: January 16, 2014

   dx.doi.org/10.1021/jp410198r | J. Phys. Chem. C 2014, 118, 2507−2517

al. reported a template-free approach for the preparation of N-doped hollow carbon microspheres by direct pyrolysis of solid melamine−formaldehyde resin spheres.[26] Although such hollow carbon spheres possessed the specific surface area of 753 m^2/g, the type-I isotherm curve obviously indicated that most of the surface area was contributed from the microporous pores, which was useless for the electrolyte ions adsorption as electrode materials. What's more, it is hard to tune nitrogen doping amount through the direct pyrolysis of N-containing polymer because the N/C ratio is fixed before the polymerization process. Later, Guo et al. reported the synthesis of N and B codoped porous carbon through the self-assembly of poly(benzoxazine-*co*-resol) with ionic liquid $C_{16}mimBF_4$.[25] However, only limited nitrogen content (~1.2 wt %) was doped by using this method, and it is difficult to obtain ordered meso-structure carbon although the soft-template F127 was employed in the synthesis. The ordered meso-structure is a critical factor in order to achieve high surface area and facilitate the ions transportation. Based on the literature referring in situ synthesis approach, tunable N-doped carbon with maintaining of ordered meso-structure was seldom synthesized, and this situation will inevitably hinder their large-scale production.

To this end, we herein develop an integrated and facile strategy to fabricate N-doped mesoporous carbon (NC) by using melamine resin as nitrogen source and phenolic resin as carbon source. The melamine resin was chosen as nitrogen source because of its large N content and high reactivity of amino group. Besides, melamine resin is an inexpensive and commercially available triazine polymer which is normally used in plastic, medicinal, organic coatings, and paper industries.[26,27] With the aim of maintaining ordered mesoporous structure and high carbon yield, melamine resin was modified by phenolic resin (serving as carbon source) through the conjunction of −NH− groups with carbon atoms. Two promising aspects of such NC include the potential to maintain morphology and ordered mesostructure after introducing nitrogen and the straightforward in situ mechanism for the incorporation of nitrogen atoms into the carbon framework. Additionally, the N-doping amount can be easily tuned by controlling the mass ratio of N-precursor and C-precursor before the polymerization process. In order to further enhance the electrochemical performance of such N-doped carbon material, 2D carbon framework of graphene sheets with high electronic conductivity were used as a doping matrix. In this N-doped carbon decorated graphene (NG), each graphene sheet was fully covered with a layer of N-doped mesoporous carbon. This kind of doping can be thought of as a "indirect" doping approach without destroying the excellent conductivity of graphene through maintaining the integrity of graphene sheets. As compared to the pure mesoporous carbon materials, the NC and NG reported in this work exhibited great potential as an efficient electrode material for supercapacitor with higher specific capacitance and excellent rate performance. Furthermore, all of the precursors used in the experiment are commercially available and suitable for scale-up production.

2. EXPERIMENT PROCEDURES

Chemicals. Graphene oxide (flake size: 0.5−5 um) was obtained from Graphene Supermarket. Melamine and phenol were purchased from Sigma-Aldrich. Formaldehyde solution (37 wt % in water) and Pluronic F127 (M_{av} = 12 000 g/mol) were purchased from Sigma. Ethanol (99.0%) and sodium hydroxide (NaOH) were obtained from Merck. All chemicals were used as received without any further purification.

Preparation of Nitrogen-Doped Mesoporous Carbon (NC), Highly Nitrogen-Doped Carbon (NC−H), and Mesoporous Carbon (MC). Nitrogen-doped mesoporous carbon (NC) was prepared through aqueous hydrothermal route. In a typical synthesis of NC, 1.2 g of melamine and 0.9 g of phenol were melted at 40 °C, and 22.5 mL of 0.1 M NaOH aqueous solution was added slowly to the round-bottom flask with continuous stirring. Ten milliliters of formalin aqueous solution (37 wt %) was added dropwise, and the reaction mixture was stirred at 70 °C for 1 h. Then 22.5 mL of well-dissolved F127 aqueous solution (containing 1.44 g of F127) was added, and the reaction mixture was stirred at 70 °C for 2 h. Subsequently 150 mL of DI water was added to the mixture. The reaction was kept at 70 °C for 16 h without nitrogen protection. After the mixture was cooled to room temperature, around 200 mL of dark-pink solution was obtained as stock solution. For the preparation of NC−H, the amount of the monomer of phenol, melamine, and formalin aqueous are 0.6 g, 1.2 g, and 10 mL, respectively. The other parameters are the same as those with the fabrication of NC. The synthesis of MC can be found in our previous work.[28]

In the second step, 50 mL of as-prepared stock solution was transferred to an autoclave after setting the pH value to 9. The autoclave was heated to 180 °C for 7 h. The product was collected, followed by centrifugation and washing with ethanol three times and drying in freeze-drying equipment.

The calcination was carried out in two steps. First, the sample was heated to 420 °C (heating rate of 2 °C/min) in nitrogen environment and kept for 30 min to remove the template in this process.[28] Second, the sample was continuously heated to 600 °C (heating rate of 2 °C/min) and kept for 1.5 h to carbonize the product.

Preparation of with Nitrogen-Doped Carbon Decorated Graphene (NG). The synthesis procedure of NG is similar to that of NC−H. It is the same procedure as in the first step of prepolymerization to obtain the NC−H stock solution.

In the second step, 20 mL of as-prepared NC−H stock solution, 20 mL of 2 mg/mL graphene oxide aqueous solution, and 10 mL of deionized water were well mixed and stirred overnight. The mixture was subsequently transferred to an autoclave after setting the pH value to 9. The autoclave was heated to 180 °C for 7 h. The product was collected, followed by centrifugation and washing with ethanol three times and drying in freeze-drying equipment. The calcination procedure is same as that with NC.

Characterization. The morphologies of the obtained samples were examined by using scanning electron microscopy (SEM; Zeiss Supra 40 FE). All transmission electron microscopy (TEM) images were obtained by using a JEOL 100CX instrument (200 kV). Samples were prepared by dripping on carbon-coated copper grids followed by drying at room temperature. The X-ray photoelectron spectroscopy (XPS) spectra were taken by using an Axis Ultra DLD X-ray photoelectron spectrophotometer equipped with an Al K_α X-ray source (1486.69 eV). N_2 sorption isotherms were measured on the Surface Area and Porosity Analyzer (ASAP 2020). Before the measurement, all samples were degassed at 120 °C for more than 5 h. The specific surface area was calculated by using the Brunauer−Emmett−Teller (BET) method. The pore volume and pore size distributions were derived from the adsorption branches of isotherms using the density functional

dx.doi.org/10.1021/jp410198r | J. Phys. Chem. C 2014, 118, 2507−2517

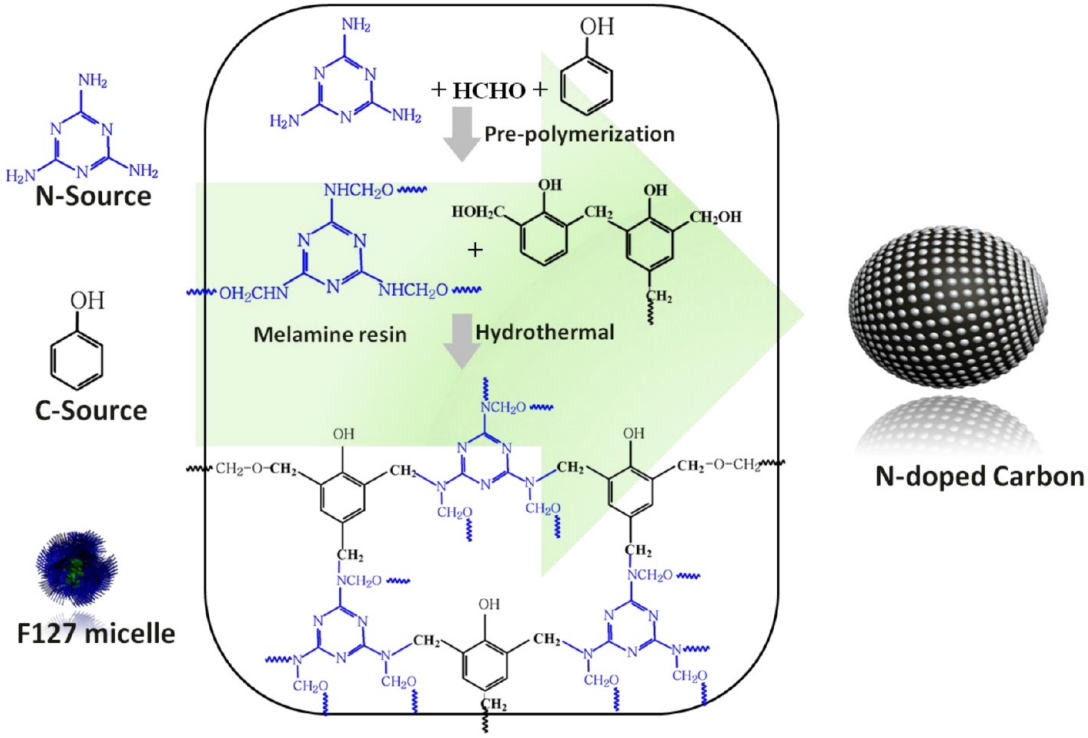

Figure 1. Schematic illustration of the general strategies to prepare nitrogen-doped mesoporous carbon.

theory (DFT) model. Fourier transform infrared (FT-IR) spectra were recorded on a Varian 3100 FT-IR (Excalibur series) spectrophotometer. Samples were prepared by casting pellets from sample/KBr mixtures. Sixty-four scans were signal-averaged with a resolution of 4 cm^{-1} at room temperature.

Electrochemical Measurements. The working electrode was prepared by mixing the 95 wt % active materials with 5 wt % poly(tetrafluoethylene) (PTFE) binder in ethanol. The homogeneous slurry of the mixture was painted between two pieces of nickel foam with an area of 1 cm^2 and followed by pressing under 15 MPa. The mass loading of the active material was in the range of 5−8 mg. The cyclic voltammetry (CV), galvanostatic charge−discharge, and electrochemical impedance spectroscopy (EIS) were performed on the electrochemical analyzer (Solartron S1 1287) under ambient condition. These electrochemical measurements were carried out by using both three-electrode and two-electrode cells. In the three-electrode system, platinum wire was used as the counter electrode and Hg/Hg_2Cl_2 as the reference electrode. Six molar KOH aqueous solutions were used as electrolyte. The two-electrode supercapacitor consisted of two symmetric working electrodes with two-layer filter paper as a separator. The total capacitance of a supercapacitor was calculated from the galvanostatic discharge process according to the following equation: $C_{total} = I \times \Delta t/(\Delta V \times m)$, where I is the discharge current (A), Δt is the discharge time (S), ΔV is the voltage change (V) excluding the IR drop during the discharge process, and m is the total mass of the active material. The electrochemical impedance spectroscopy measurement of the supercapacitor was performed with an amplitude of 10 mV in the frequency range from 100 kHz to 10 mHz.

3. RESULTS AND DISCUSSION

A schematic illustration for preparation of N-doped mesoporous carbon spheres (NCs) is presented in Figure 1. For the precursors listed on the left side of Figure 1, melamine served as monomer of nitrogen source and phenol served as monomer of carbon source, while block copolymer F127 was used as a soft-template. During the prepolymerization process illustrated in the middle of Figure 1, F127 micelles were encapsulated by low-molecular-weight melamine/phenolic resin under the drive of hydrogen bonding to form the composite monomicelles. Upon the following hydrothermal process, the composite monomicelles were further self-assembled and solidified into composite spheres with diameter around 200 nm through cross-linking of melamine resin and phenolic resin. By increasing the amount of N source introduced, highly N-doped mesoporous carbon (NC−H) could be formed with larger particle size.

The transmission electron microscopy (TEM) image of NCs was shown in Figure 2a. The NCs were in spherical morphology and had an average particle size of 200 nm. Also, high-resolution TEM (HRTEM) image clearly showed their mesostructure with the estimated pore size of 6 nm. By increasing the amount of N source melamine resin introduced, the morphology of NC−H was transformed to larger particles as well as more ordered structure (Figure 2b). It is supposed that the morphology evolution is related to the interaction between triazine-riched micelles during the self-assembly process. In detail, the NC−H samples offered content of triazine groups two times higher than NC samples, which will significantly contribute the hydrogen bonding during the self-assembly process. Such stronger hydrogen bonding will ultimately facilitate self-assembly of particles and result in larger ones. As shown in Figure 2b, the TEM image of NC−H clearly showed their ordered mesostructure, and the pore size is estimated to be 8.2 nm from the inset HRTEM image.

In order to demonstrate the nature of the doping in the as-obtained carbonaceous materials, elemental mapping images of carbon, nitrogen, and oxygen were conducted (Figure 2c). As

dx.doi.org/10.1021/jp410198r | J. Phys. Chem. C 2014, 118, 2507−2517

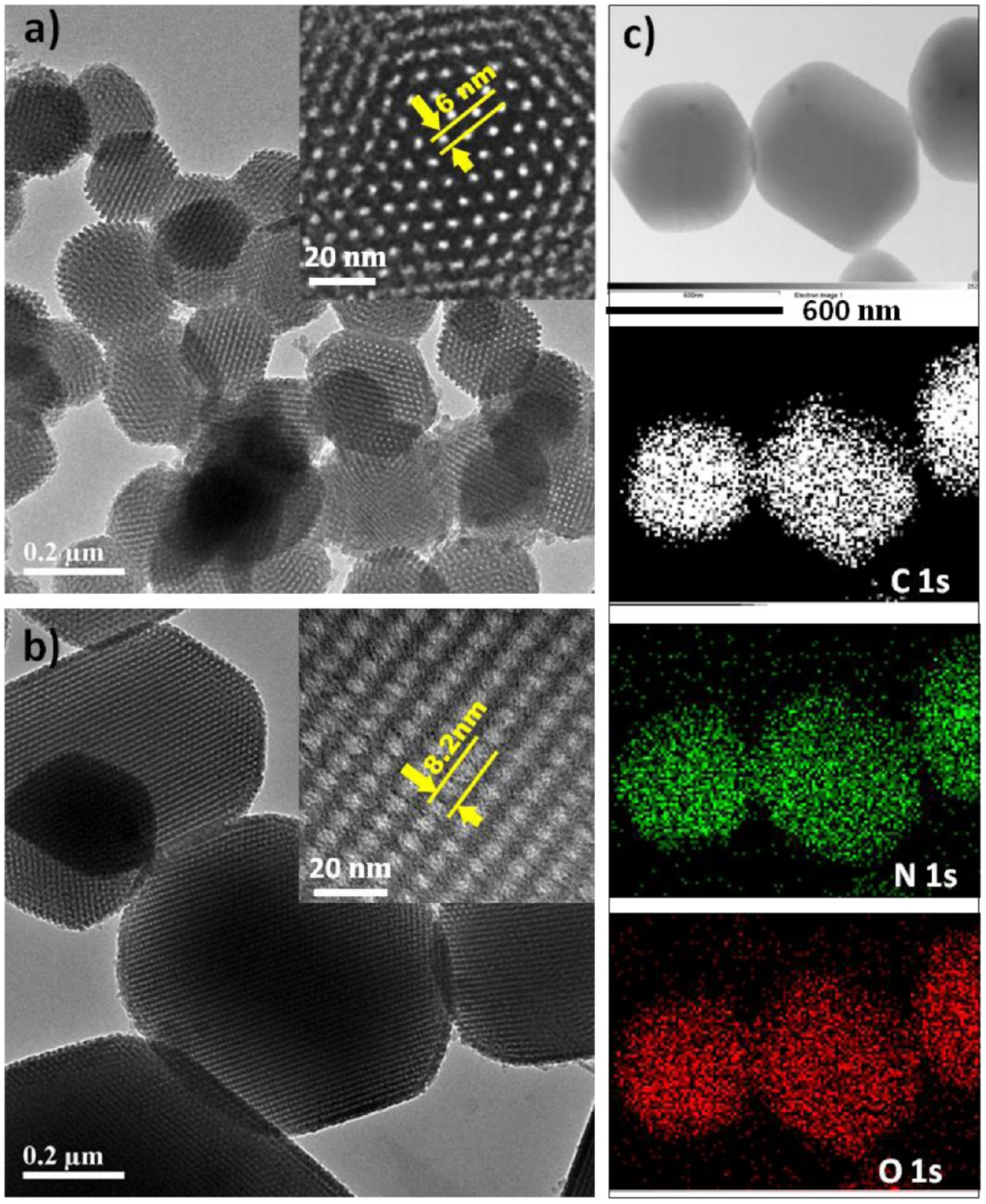

Figure 2. TEM images of (a) NC (inset is the respective HRTEM image labeled with average pore diameter); (b) highly N-doped carbon (NC−H); (c) NC−H TEM mapping images with the elements of carbon, nitrogen, and oxygen, respectively.

expected, nitrogen and oxygen atoms were homogeneously dispersed in the spherical carbon matrix. The exact content of these heteroatoms would be determined by using elemental analysis and X-ray photoelectron spectroscopy (XPS) below. According to the literature, both the nitrogen and oxygen functional group in electrode materials can enhance the energy density and specific power of capacitor.[10] The mechanism of oxygen is also to allow electrode materials possessing pseudocapacitance, which is the same strategy as with nitrogen.

In order to evaluate the nitrogen doping degree and nitrogen bonding configurations, XPS characterizations were carried out on the N-doped carbon samples. For the sake of comparison, pure mesoporous carbon (MC) without N doping was also synthesized, and the corresponding TEM image is shown in Figure S1of the Supporting Information. As shown in Figure 3a, the XPS spectrum of MC sample showed only the presence of carbon and oxygen elements. However, the XPS spectra for NC−H without calcination treatment clearly showed the incorporation of nitrogen atoms within melamine resin, which could be further proved from the Fourier transform infrared spectroscopy (FTIR) results below. According to the XPS quantitative analysis, the N/C weight ratio of NC−H without calcination is 0.36. This kind of nitrogen-doped polymer composite was subsequently annealed up to 600 °C, and the N/C ratios of NC and NC−H were decreased to 0.053 and 0.064 owing to the thermal loss of N-containing functional groups under such high temperature. In contrast, the elemental analysis results (Table 2) revealed that the N/C ratio of NC and NC−H samples carbonized at 600 °C range from 0.055 to 0.07, associated with 4.12 and 5.46 wt % nitrogen content, respectively. Combination of the elemental analysis and the XPS results (Table 2) suggested that the bulk N-content of the carbon was slightly higher than the surface content. The high-resolution C 1s XPS spectrum of NC−H (Figure 3b) was

dx.doi.org/10.1021/jp410198r | J. Phys. Chem. C 2014, 118, 2507−2517

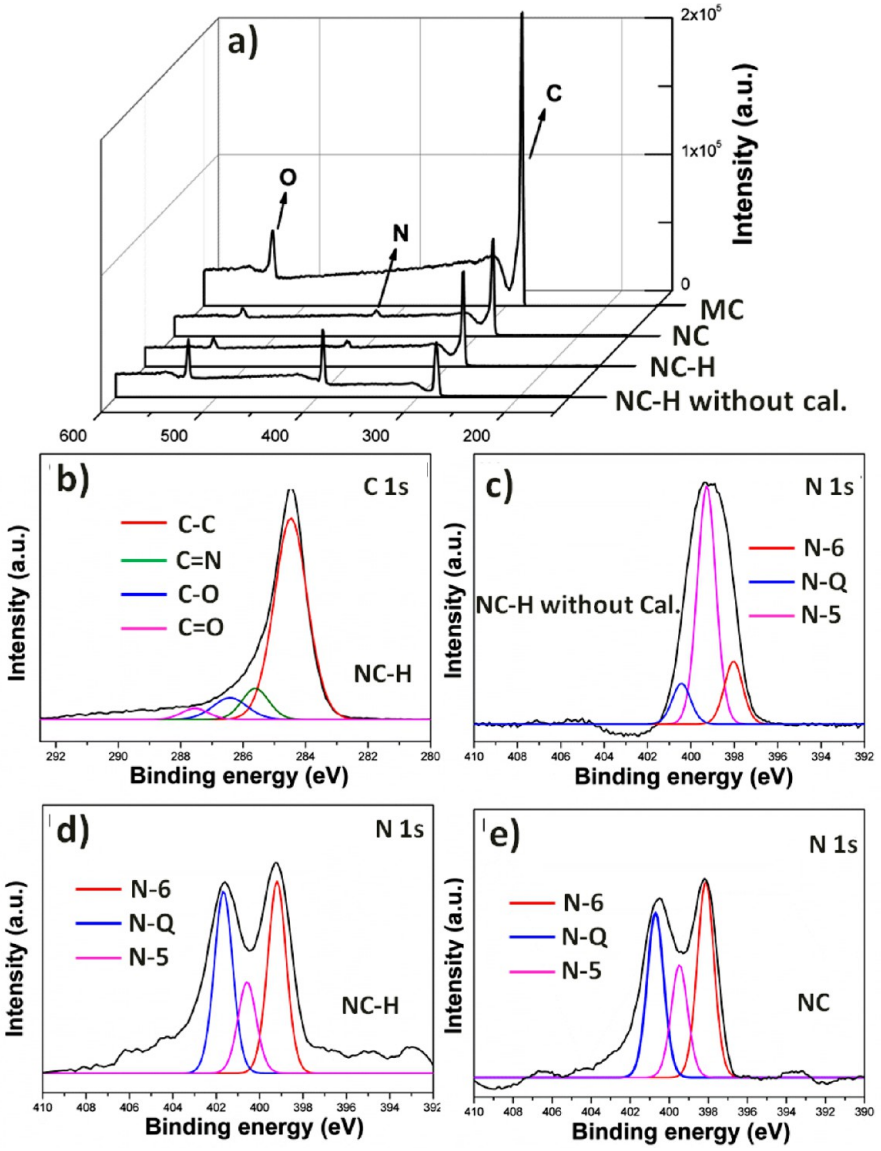

Figure 3. (a) XPS survey spectra of various mesoporous carbon; (b) carbon core level XPS spectra of NC−H; N core level XPS spectra of (c) NC−H without calcination, (d) NC−H, and (e) NC.

deconvoluted into four peaks (colored lines) with different relative carbon contents: sp^2-bonded carbon at 284.5 eV (C−C, 78.25%), carbon nitrogen double-bond at 285.8 eV (C═N, 9.63%), epoxy/hydroxyls at 286.4 eV (C−O, 8.69%), and carbonyls at 288.4 eV (C═O, 3.43%). The low C−O, C═O, and C═N bonding configurations reveal that most of the oxygen and nitrogen groups have been removed, and the graphite carbon network was partially restored.[29]

Similarly, the bonding configurations of nitrogen atoms in NC samples were characterized by the high-resolution N 1s spectra. Figure 3c−e show the N 1s spectra of selected samples, which were fitted into three peaks: pyridinic (N-6) at 398 eV, pyrrolic/pyridine (N-5) at 399.7 eV, and quaternary nitrogen (N-Q) at 400.7 eV.[10,30] For example, the NC−H without calcination (Figure 3c) shows the dominant peak at 399.7 eV (69.7%) corresponding to N atoms within the hexagonal ring of the melamine resin.[31] The detailed percentage of each component is shown in Table 1. Upon 600 °C annealing treatment, the N-5 peak becomes much weaker and its proportion is obviously smaller (19.6%) than corresponding nonannealing sample, while the N-Q and N-6 (Figure 3d) appear much stronger. These results suggest that N atoms within the hexagonal ring of melamine resin are converted into two types of nitrogen (N-Q and N-6) during the carbonization process.[30,32] Figure 3e shows the N 1s spectra of NC with the detailed component of N-6 (41.5%), N-5 (23.7%), and N-Q (34.8%). It is reported that the N at the edge of graphite plane (N-5, N-6) is more active than that located in the middle of graphite plane (N-Q).[33−35] Notably, the percentages of N on

Table 1. Approximate Distribution of N Functional Groups Obtained by Fitting the N 1s Core Level XPS Spectra for the NC, NC−H, and NC−H without Calcination

	% of total N 1s		
functional groups	N-Q	N-5	N-6
B.E. (eV)	400.7	399.7	398
NC	34.8	23.7	41.5
NC−H	39.1	19.6	41.3
NC−H without cal.	11.9	69.7	18.4

dx.doi.org/10.1021/jp410198r | J. Phys. Chem. C 2014, 118, 2507−2517

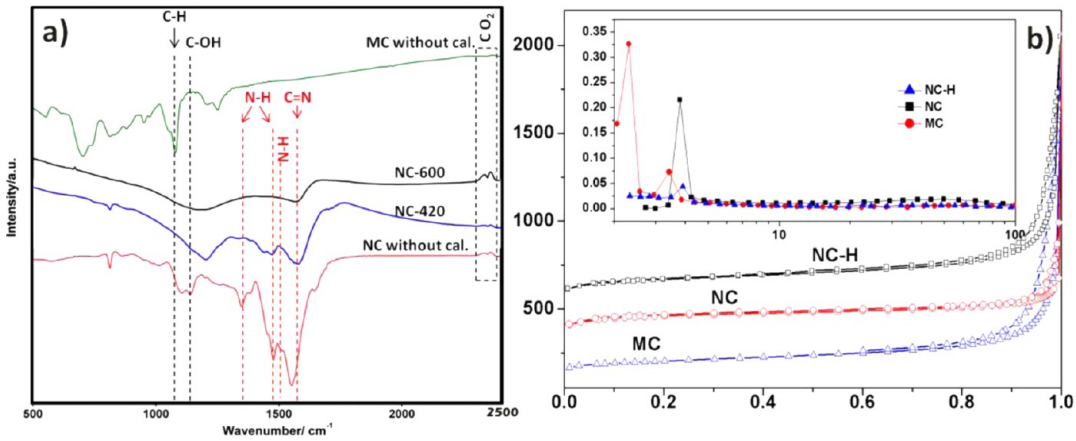

Figure 4. (a) FT-IR spectra of nitrogen-doped carbon materials; (b) N_2 adsorption−desorption isothermals and (inset) pore-size distributions of MC, NC, and NC−H.

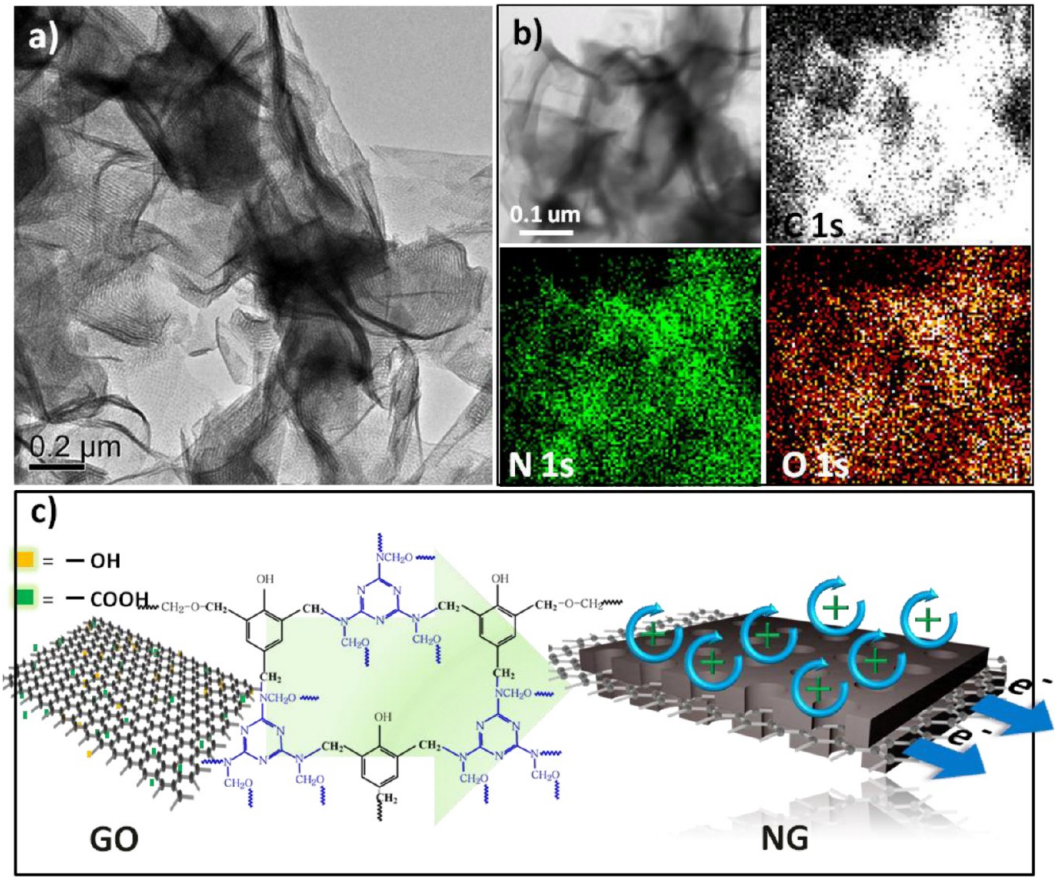

Figure 5. (a) TEM images of NG; (b) TEM mapping images of NG with the elements of carbon, nitrogen, and oxygen, respectively. (c) Scheme illustrating formation of N-doped graphene associated with rapid electrons transport and electrolyte ions effectively accumulated beside the N-doped porous carbon layer.

edge in our sample of NC and NC−H are very high, 65.2% in NC and 60.9% in NC−H.

The evolution of the chemical composition of the obtained carbon materials was further characterized by FTIR, as shown in Figure 4a. For the pure mesoporous carbon before calcination, only some carbon-based functional groups such as C−H (1070 cm^{-1}) and C−OH (1100 cm^{-1}) can be detected. In contrast, the N-doped mesoporous carbons obtained at different annealing temperatures show similar FTIR spectra and similar absorption peaks to one another (420 and 600 represent annealing temperature: Celsius degree). For example, the bands at ca. 1530, 1392, and 1262 cm^{-1} can be assigned to the presence of the N−H bonding. Nitrogen in the form of C═N bonding (ca. 1645 cm^{-1}) was also observed. Hence, the FTIR analysis confirms the existence of N-containing functional groups in the as-obtained composite materials.

The specific surface areas of the N-doped carbons were characterized by using isothermal N_2 adsorption−desorption method. For the convenience of comparison, pure MC was also

dx.doi.org/10.1021/jp410198r | J. Phys. Chem. C 2014, 118, 2507−2517

Table 2. Physicochemical Characterization of Various Carbon-Based Materials

sample	BET surface area (m^2/g)[a]	total pore volume (cm^3/g)	average pore size (nm)[b]	C[c] (wt %)	N[c] (wt %)	N/C ratio[c]	specific capacitance -III (F/g)[d]	specific capacitance -II (F/g)[e]
MC	1056	1.14	5.5	84.38	–	–	127	–
NC	962	0.84	6.9	75.00	4.12	0.055	222.9	–
NC–H	850	0.81	8.6	78.12	5.46	0.070	238	38.2
NG	588	0.56	11.1	75.75	6.63	0.088	289	39.5

[a]Calculated by the BET model from the adsorption branches of the isotherms. [b]Calculated by the multipoint DFT model from desorption data. [c]Data obtained from combustion elemental analysis. [d]Calculated from the galvanostatic discharge at the current density of 0.2 A/g (based on three-electrode system). [e]Calculated from the galvanostatic discharge at the current density of 0.5 A/g (based on total mass of the active material in a two-electrode symmetric supercapacitor).

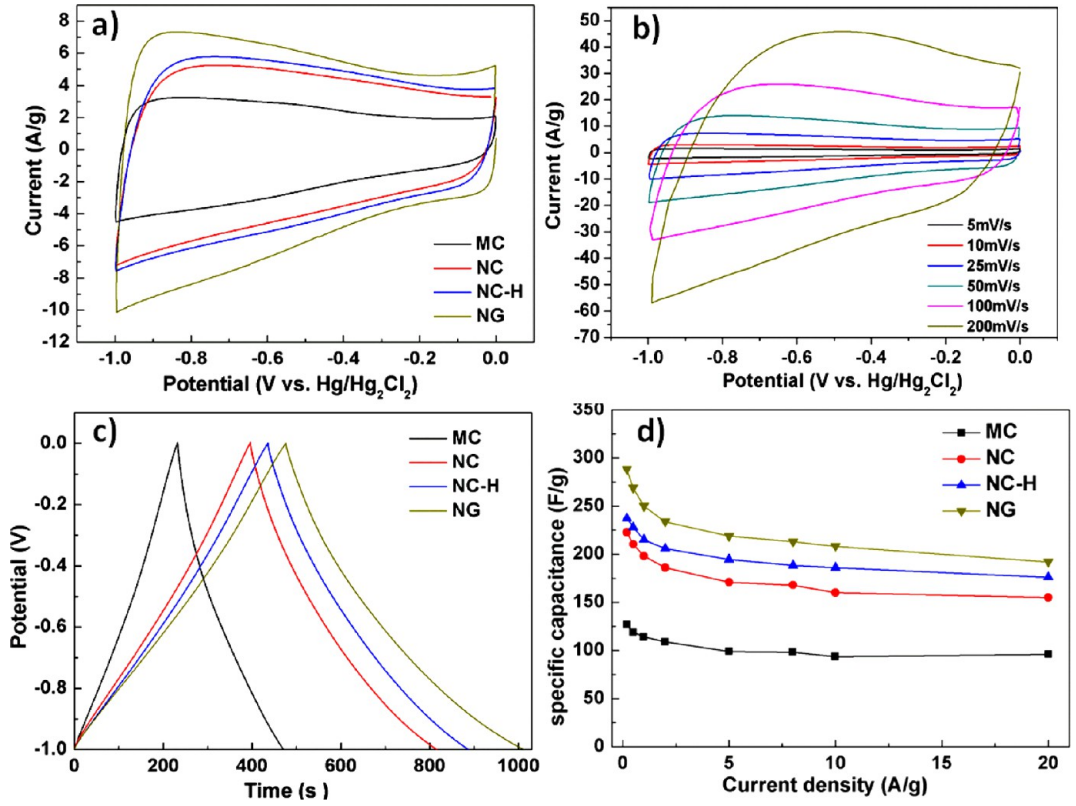

Figure 6. Electrochemical performance of carbon-based composite in a three-electrode system. Cyclic voltammograms of (a) various N-doped carbon electrodes measured at the scan rate of 25 mV/s and (b) NG electrode measured at different scan rates. (c) Galvanostatic charge–discharge curves of various N-doped carbon electrodes at a current density of 0.5 A/g. (d) Variation of specific capacitance of various N-doped carbon electrodes at different current densities.

prepared at the same calcination condition and its specific surface area was measured as a reference. As can be seen from Figure 4b, all the N_2 adsorption–desorption isotherms of N-doped carbon showed the cross-curves between type-I and type-IV curves, suggesting the presence of micro/mesopores in these carbon-based electrode materials. In particular, the isotherm of NC and NC–H displayed H1 hysteresis loop at a relatively high pressure, which revealed that most of the pores were formed by regularly shaped mesopores with narrow size distribution. The pore size distributions (Figure 4b inset) were calculated using the density functional theory (DFT) model from the desorption branches of the isotherms. The BET surface area and average pore size of MC (Table 2) were 1056 m^2/g and 5.5 nm, respectively. After introduction of nitrogen atoms, the surface area of NC was decreased to 962 m^2/g, but the average pore size was increased to 6.9 nm. By further doping nitrogen to 5.46 wt %, the surface area of NC–H was continuously decreased to 850 m^2/g due to the larger pore size of 8.6 nm. It is supposed that the evolution of pore size is due to the relatively easy elimination of triazine ring. The contributions of pores formation are the eliminations of primary template F127 and subordinately surrounding cross-link polymer during the carbonization process, which is shown in Figure S2 of the Supporting Information. As we know, the triazine ring in NC or NC–H is less stable than the benzene ring in MC under high temperature. Consequently, it is reasonable to understand that the pore size of NC or NC–H is larger than that of MC. Although the specific surface areas of N-doped carbon samples were relatively lower as compared to pure MC, the larger pores in N-doped carbons were much more favorable for ion diffusion at high sweep rate than those in MC.[36] This would ultimately lead to the more efficient utilization of specific surface area of electrode materials.

In order to verify the feasibility of such N-doping strategy and achieving higher electrochemical performance, 2D carbon framework of graphene was introduced as carbon matrix to

dx.doi.org/10.1021/jp410198r | J. Phys. Chem. C 2014, 118, 2507–2517

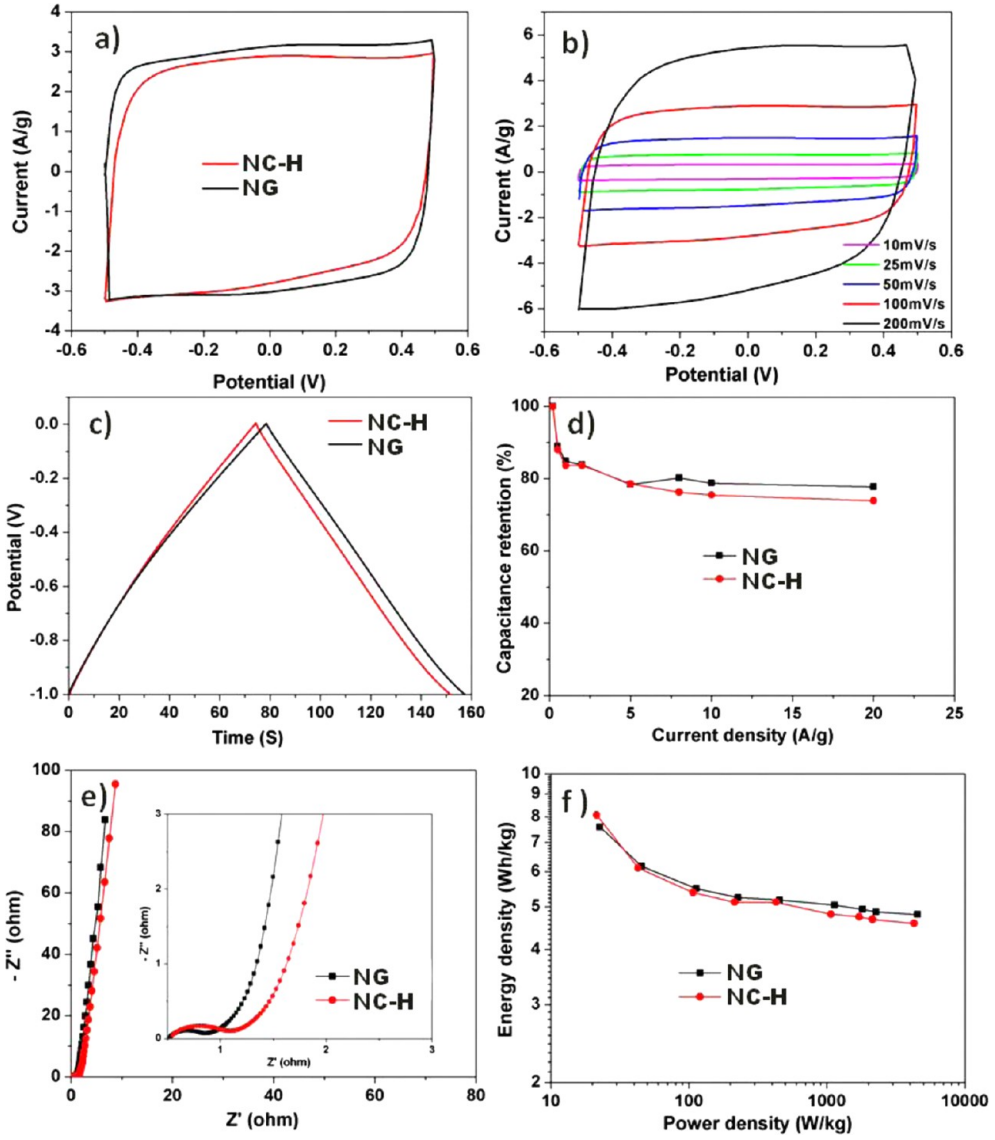

Figure 7. Electrochemical performance of carbon-based composites in a two-electrode system. Cyclic voltammograms (a) measured at the scan rate of 25 mV/s and (b) NG−H electrode measured at different scan rates. (c) Galvanostatic charge−discharge curves at a current density of 0.5 A/g. (d) Capacitance retention against current density of N-doped carbon electrodes. (e) Electrochemical impedance spectra under the influence of an ac voltage of 10 mV. (f) Ragone plots of N-doped carbon supercapacitor.

obtain NG. Interestingly, the as-obtained NG exhibited some unique structures as compared to the commonly reported nitrogen-doped graphene. As can be seen in TEM image of Figure 5a, the N-doped mesoporous carbon layer was attached in between the graphene sheets, and there were numerous mesopores on the surface of graphene sheets. From the observation of low-magnification TEM shown in Figure S3 of the Supporting Information, numerous open channels were formed in between the graphene sheets in the presence of these mesoporous carbon layers which would greatly facilitate access of electrolyte. The TEM mapping results (Figure 5b) suggested that nitrogen and oxygen atoms were homogeneously dispersed in the carbon matrix. The exact content of these heteroatoms as well as some other physicochemical characterization results are provided in Table 2. Notably, the surface area of NG was only 588 m^2/g because of the introduction of graphene sheets. However, the average pore size was increased to 11.1 nm owing to the presence of a large amount of slitlike pores. The scheme illustration of NG formation is presented in Figure 5c: NG was fabricated by self-assembling composite monomicelles onto GO sheets under the driving of hydrogen bonding between the micelles and the functional groups of GO. After thermal treatment, the polymeric micelles were converted into N-doped mesoporous carbon layer which was then firmly attached onto the graphene sheets. The scheme illustration of NG in Figure 5c also presented the rapid electrons transport and electrolyte ions effectively accumulated besides the N-doped porous carbon layer. As supposed, the thin carbon layer and optimized graphene sheet structure offer a shortened diffusion pathway for electron transportation and electrolyte penetration.[37,38] Meanwhile, the numerous mesopores and homogeneously dispersed N functional groups provide a huge accumulation place for electrolyte ions and allow a high loading amount of energy. These advantages will ultimately result in remarkable energy storage performance. Compared with the commonly reported nitrogen-doped graphene, such graphenes decorated with N-doped carbon have several advantages: there is relative ease in controlling doping amount via tuning the N-precursor amount,

dx.doi.org/10.1021/jp410198r | J. Phys. Chem. C 2014, 118, 2507−2517

the "indirectly doping" will uttermost maintain the integrity and excellent conductivity of graphene, and "sandwichlike" porous structure is able to inhibit the aggregation of the graphene sheets effectively.

In order to study the electrochemical performance of the as-made N-doped carbon samples, the cyclic voltammetry (CV) and galvanostatic charge−discharge techniques were used first in 6.0 mol/L KOH electrolyte on the basis of three-electrode (Figure 6). The pure MC obtained at the same calcination condition was also tested as reference. Figure 6a shows the CV curves of MC, NC, and NG samples at a scan rate of 25 mV/s. All the CV curves in Figure 6a exhibited roughly rectangular shape, indicating that the dominant capacitance of the electrodes was formed by EDLC. In detail, the MC sample in Figure 6a exhibited the smallest rectangular curve corresponding to the lowest capacitance among the three samples. Although the surface area of MC was the largest among the four samples, the presence of large amount of micropores (Table 2) limited ion incorporation into the electrode material. This ultimately led to inefficient utilization of specific surface area. NC, NC−H, and NG electrodes exhibited roughly rectangular shape and a few humps in these CV curves due to the combination of EDLC and pseudocapacitance. Notably, the NG possesses the largest CV curve and highest capacitance value. This high performance can be attributed to its highest N-doping content and favorable pore size distribution. The CV curves of NG electrode at various sweep rates are displayed in Figure 6b. It shows increased current response with the increased sweep rate, indicating a favorable capacitive behavior.[39] The CV curve of NG still remained the rectangular shape even at the high sweep rate of 200 mV/s, which was benefited from its excellent electronic conductivity. In contrast, the CV curve of MC electrode (Figure S4 of the Supporting Information) at high scan rate was significantly distorted. Such an electrochemical behavior was mainly due to the relatively large internal resistance, which was caused by the limited ion incorporation because of its relatively small pores.

The capacitive performance was further evaluated by galvanostatic charge−discharge experiment at different current densities with the same voltage windows as CV analysis. Figure 6c shows the galvanostatic charge−discharge of various carbon-based electrodes at the current density of 0.5 A/g. As can be seen, NG electrode showed the largest discharge time, whereas NC−H and NC electrodes exhibited slightly reduced discharge time. This observation suggested that NG offered the largest capacitance (268.9 F/g), followed by NC−H (228 F/g) and NC (210.4 F/g), which agreed with the trend obtained from CV results. However, the pure MC electrode only offered the capacitances of 119 F/g, respectively. Moreover, the nearly symmetric charge−discharge profiles of N-doped carbon electrodes suggested the dominant EDLC mechanism. The asymmetry is caused by the pseudocapacitive behavior of the N-containing and O-containing functional groups on the surface. Notably, the achieved capacitance value of NG is quite advantageous as compared to the most reported N-doped carbon materials at the same measurement condition (Supporting Information Table S1). For example, the capacitance of B and N codoped graphene was 239 F/g at the current density of 1 mV/s (Supporting Information ref S6). As discussed in the prior section, the high capacitance value of as-obtained NC and NG is due to the relatively large N-doping amount and optimum pore size distribution, which are favorable for ion diffusion. In order to investigate the capacitance retention of the as-obtained electrode materials at high current density, Figure 6d shows the variation of specific capacitance at different current densities. A slightly decrease in the capacitance of N-doped carbon samples was observed from the current density of 0.2−20 A/g. Furthermore, the capacitances of the three samples were maintained well under high current densities, suggesting that these electrode materials had good capacitance retention capability.

The supercapacitor performances of NC−H and NG were then investigated by symmetrical two-electrode cell setup.[40] Figure 7a shows the CV curves of electrodes at the scan rate of 25 mV/s, which exhibited a nice rectangular shape with slight humps between −0.2 and 0.2 V. This observation suggests the mechanism of dominant EDLC and subordinate pseudocapacitance. Again, the as-obtained device still maintained the rectangular shaped CV even at the high scan rate, from the CV curves at various scan rates as illustrated in Figure 7b. The triangle-like charge/discharge curves for the as-obtained capacitors in Figure 7c proved their excellent reversible capacitive behavior. In addition, the NC−H and NG capacitors delivered specific capacitances of 38.8 and 39.5 F/g at the current density of 0.5 A/g, respectively, based on the total active material mass of two electrodes. In order to study the rate capability of electrodes, the capacitance retention was calculated at various current densities (Figure 7d). In detail, the capacitance based on the symmetric NG electrode decreased from 54.5 to 34.5 F/g as the current density increased from 0.1 to 20 A/g, showing a capacitance retention as much as 78%. In contrast, slightly inferior performance of 75% initial capacitance was preserved for NC−H electrodes due to its lower electrical conductivity in the absence of graphene. The Nyquist impedance spectrum of the electrodes was also recorded from 0.01 to 100 000 Hz at open-circuit potential in order to demonstrate the internal resistance of the electrode materials. The smaller semicircle was observed for the NG capacitor (Figure 7e, inset) at high frequency, suggesting that it had relatively small charge transfer resistance.[41,42] The Ragone plots provided in Figure 7f show the relation between energy density and power output of a supercapacitor. It is noteworthy to mention that the NC−H electrode delivered a high energy density of 8.6 Wh/kg at the current density of 0.1 A/g, whereas the NG electrode only delivered 7.6 Wh/kg at the same current density. However, the energy density drops slowly from 7.6 to 5.0 Wh/kg for NG electrode as the power density increased from 23 W/kg to 4.6 kW/kg. Such superior rate performance benefits from the improved conductivity of graphene and rational sandwichlike porous nanostructure.

In addition, we demonstrated the cycling stability of NG electrode by using the continuous charge−discharge experiment at constant current density. The capacitance retention as a function of cycle number based on the three-electrode system is provided in Figure S5 of the Supporting Information. The NG electrode offered 87% capacitance retention after 4000 cycles, revealing its good cycle stability. In the result for symmetric two-electrode cell in Figure 8, it is clear that the capacitance retention is as high as 91% after 1000 cycles, which suggests its good cycling and stability behavior as well. Besides, the nearly triangular charge−discharge curves (Figure 8, inset) demonstrated that such electrodes offer stable performance and good charge propagation. Overall, the achieved superior cycling performance can be attributed to the following: uniform dispersion of molecular nitrogen groups on the graphene

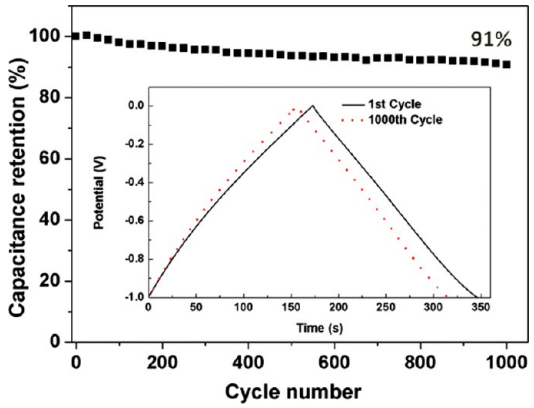

Figure 8. Cyclability of the NG electrode in a 6 mol/L KOH electrolyte. Data was obtained from a two-electrode supercapacitor by using the galvanostatic charge−discharge technique with a current density of 0.5 A/g.

surface and high reversibility and stability during the cycling process.

4. CONCLUSIONS

In summary, we demonstrated an integrated and reproducible chemical process to fabricate the N-doped mesoporous carbon and graphene by using melamine resin as the nitrogen source. The as-made NC and NG electrode materials exhibited high surface area, suitable pore size distribution, and uniformly dispersed N functional groups with tunable doping amount. These unique properties endowed them as promising electrodes for supercapacitor with superior performance. For example, on the basis of the three-electrode system, NC−H and NG electrodes could deliver the specific capacitance of 238 and 289 F/g at the current density of 0.2 A/g, respectively. The capacitance of NC−H was improved by 91.6% as compared to the pure mesoporous carbon without nitrogen doping under the current density of 0.5 A/g. The performance of the as-made electrode was also investigated by symmetrical two-electrode cell. The results revealed that the as-made electrodes offered excellent rate capability (ca. 78% retention as the current density increased from 0.1 to 20 A/g) and superior cycling performance (ca. 91% retention after 1000 cycles). These results demonstrate that the nitrogen-doped carbon/graphene presented here is quite a promising candidate of an electrode as superior performance supercapacitor.

■ ASSOCIATED CONTENT

Supporting Information

Figures S1−S5 and Table S1 as described in the text. This material is available free of charge via the Internet at http://pubs.acs.org.

■ AUTHOR INFORMATION

Corresponding Author

*Tel.: +65 65164655. E-mail address: msexuejm@nus.edu.sg.

Notes

The authors declare no competing financial interest.

■ REFERENCES

(1) Pan, H.; Li, J.; Feng, Y. P. Carbon Nanotubes for Supercapacitor. *Nanoscale Res. Lett.* **2010**, *5*, 654−668.
(2) Zhang, L.; Zhao, X. S. Carbon-Based Materials as Supercapacitor Electrodes. *Chem. Soc. Rev.* **2009**, *38*, 2520−2531.
(3) Barbieri, O.; Hahn, M.; Herzog, A.; Kotz, R. Capacitance Limits of High Surface Area Activated Carbons For Double Layer Capacitors. *Carbon* **2005**, *43*, 1303−1310.
(4) Gamby, J.; Taberna, P. L.; Simon, P.; Fauvarque, J. F.; Chesneau, M. Studies and Characterisations of Various Activated Carbons Used for Carbon/Carbon Supercapacitors. *J. Power Sources* **2001**, *101*, 109−116.
(5) Babel, K.; Jurewicz, K. KOH Activated Carbon Fabrics as Supercapacitor Material. *J. Phys. Chem. Solids* **2004**, *65*, 275−280.
(6) Frackowiak, E. Carbon Materials for Supercapacitor Application. *Phys. Chem. Chem. Phys.* **2007**, *9*, 1774−1785.
(7) Rakhi, R. B.; Chen, W.; Cha, D.; Alshareef, H. N. Nanostructured Ternary Electrodes for Energy-Storage Applications. *Adv. Energy Mater.* **2012**, *2*, 381−389.
(8) Chen, Z.; Ren, W.; Gao, L.; Liu, B.; Pei, S.; Cheng, H.-M. Three-Dimensional Flexible and Conductive Interconnected Graphene Networks Grown by Chemical Vapour Deposition. *Nat. Mater.* **2011**, *10*, 424−428.
(9) Zhai, Y.; Dou, Y.; Zhao, D.; Fulvio, P. F.; Mayes, R. T.; Dai, S. Carbon Materials for Chemical Capacitive Energy Storage. *Adv. Mater.* **2011**, *23*, 4828−4850.
(10) Hulicova-Jurcakova, D.; Seredych, M.; Lu, G. Q.; Bandosz, T. J. Combined Effect of Nitrogen- and Oxygen-Containing Functional Groups of Microporous Activated Carbon on Its Electrochemical Performance in Supercapacitors. *Adv. Funct. Mater.* **2009**, *19*, 438−447.
(11) Hulicova-Jurcakova, D.; Kodama, M.; Shiraishi, S.; Hatori, H.; Zhu, Z. H.; Lu, G. Q. Nitrogen-Enriched Nonporous Carbon Electrodes with Extraordinary Supercapacitance. *Adv. Funct. Mater.* **2009**, *19*, 1800−1809.
(12) Jeong, H. M.; Lee, J. W.; Shin, W. H.; Choi, Y. J.; Shin, H. J.; Kang, J. K.; Choi, J. W. Nitrogen-Doped Graphene for High-Performance Ultracapacitors and the Importance of Nitrogen-Doped Sites at Basal Planes. *Nano Lett.* **2011**, *11*, 2472−2477.
(13) Li, X.; Wang, H.; Robinson, J. T.; Sanchez, H.; Diankov, G.; Dai, H. Simultaneous Nitrogen Doping and Reduction of Graphene Oxide. *J. Am. Chem. Soc.* **2009**, *131*, 15939−15944.
(14) Wen, Z.; Wang, X.; Mao, S.; Bo, Z.; Kim, H.; Cui, S.; Lu, G.; Feng, X.; Chen, J. Crumpled Nitrogen-Doped Graphene Nanosheets with Ultrahigh Pore Volume for High-Performance Supercapacitor. *Adv. Mater.* **2012**, *24*, 5610−5616.
(15) Zhong, M.; Kim, E. K.; McGann, J. P.; Chun, S.-E.; Whitacre, J. F.; Jaroniec, M.; Matyjaszewski, K.; Kowalewski, T. Electrochemically Active Nitrogen-Enriched Nanocarbons with Well-Defined Morphology Synthesized by Pyrolysis of Self-Assembled Block Copolymer. *J. Am. Chem. Soc.* **2012**, *134*, 14846−14857.
(16) Lu, A.; Kiefer, A.; Schmidt, W.; Schüth, F. Synthesis of Polyacrylonitrile-Based Ordered Mesoporous Carbon with Tunable Pore Structures. *Chem. Mater.* **2003**, *16*, 100−103.
(17) Li, L.; Liu, E.; Li, J.; Yang, Y.; Shen, H.; Huang, Z.; Xiang, X.; Li, W. A Doped Activated Carbon Prepared from Polyaniline for High Performance Supercapacitors. *J. Power Sources* **2010**, *195*, 1516−1521.
(18) Vinu, A.; Srinivasu, P.; Mori, T.; Sasaki, T.; Asthana, A.; Ariga, K.; Hishita, S. Novel Hexagonally Ordered Nitrogen-Doped Mesoporous Carbon from SBA-15/Polyaniline Nanocomposite. *Chem. Lett.* **2007**, *36*, 770−771.
(19) Chen, L.-F.; Zhang, X.-D.; Liang, H.-W.; Kong, M.; Guan, Q.-F.; Chen, P.; Wu, Z.-Y.; Yu, S.-H. Synthesis of Nitrogen-Doped Porous Carbon Nanofibers as an Efficient Electrode Material for Supercapacitors. *ACS Nano* **2012**, *6*, 7092−7102.
(20) Yang, C.-M.; Weidenthaler, C.; Spliethoff, B.; Mayanna, M.; Schüth, F. Facile Template Synthesis of Ordered Mesoporous Carbon with Polypyrrole as Carbon Precursor. *Chem. Mater.* **2004**, *17*, 355−358.
(21) Fuertes, A. B.; Centeno, T. A. Mesoporous Carbons with Graphitic Structures Fabricated by Using Porous Silica Materials as

Templates and Iron-Impregnated Polypyrrole as Precursor. *J. Mater. Chem.* **2005**, *15*, 1079−1083.
(22) Wei, L.; Sevilla, M.; Fuertes, A. B.; Mokaya, R.; Yushin, G. Polypyrrole-Derived Activated Carbons for High-Performance Electrical Double-Layer Capacitors with Ionic Liquid Electrolyte. *Adv. Funct. Mater.* **2012**, *22*, 827−834.
(23) Lee, J. H.; Park, N.; Kim, B. G.; Jung, D. S.; Im, K.; Hur, J.; Choi, J. W. Restacking-Inhibited 3D Reduced Graphene Oxide for High Performance Supercapacitor Electrodes. *ACS Nano* **2013**, *7*, 9366−9374.
(24) Kailasam, K.; Jun, Y.-S.; Katekomol, P.; Epping, J. D.; Hong, W. H.; Thomas, A. Mesoporous Melamine Resins by Soft Templating of Block-co-Polymer Mesophases. *Chem. Mater.* **2009**, *22*, 428−434.
(25) Guo, D.-C.; Mi, J.; Hao, G.-P.; Dong, W.; Xiong, G.; Li, W.-C.; Lu, A.-H. Ionic Liquid C16mimBF4 Assisted Synthesis of Poly(benzoxazine-*co*-resol)-Based Hierarchically Porous Carbons with Superior Performance in Supercapacitors. *Energy Environ. Sci.* **2013**, *6*, 652−659.
(26) Ma, F.; Zhao, H.; Sun, L.; Li, Q.; Huo, L.; Xia, T.; Gao, S.; Pang, G.; Shi, Z.; Feng, S. A Facile Route for Nitrogen-Doped Hollow Graphitic Carbon Spheres with Superior Performance in Supercapacitors. *J. Mater. Chem.* **2012**, *22*, 13464−13468.
(27) Hulicova, D.; Kodama, M.; Hatori, H. Electrochemical Performance of Nitrogen-Enriched Carbons in Aqueous and Non-Aqueous Supercapacitors. *Chem. Mater.* **2006**, *18*, 2318−2326.
(28) Li, M.; Xue, J. Ordered Mesoporous Carbon Nanoparticles with Well-Controlled Morphologies from Sphere to Rod via a Soft-Template Route. *J. Colloid Interface Sci.* **2012**, *377*, 169−75.
(29) Sheng, Z.-H.; Shao, L.; Chen, J.-J.; Bao, W.-J.; Wang, F.-B.; Xia, X.-H. Catalyst-Free Synthesis of Nitrogen-Doped Graphene via Thermal Annealing Graphite Oxide with Melamine and Its Excellent Electrocatalysis. *ACS Nano* **2011**, *5*, 4350−4358.
(30) Su, F.; Poh, C. K.; Chen, J. S.; Xu, G.; Wang, D.; Li, Q.; Lin, J.; Lou, X. W. Nitrogen-Containing Microporous Carbon Nanospheres with Improved Capacitive Properties. *Energy Environ. Sci.* **2011**, *4*, 717−724.
(31) Kapteijn, F.; Moulijn, J. A.; Matzner, S.; Boehm, H. P. The Development of Nitrogen Functionality in Model Chars during Gasification in CO_2 and O_2. *Carbon* **1999**, *37*, 1143−1150.
(32) Shrestha, S.; Mustain, W. E. Properties of Nitrogen-Functionalized Ordered Mesoporous Carbon Prepared Using Polypyrrole Precursor. *J. Electrochem. Soc.* **2010**, *157*, B1665−B1672.
(33) Ania, C. O.; Khomenko, V.; Raymundo-Piñero, E.; Parra, J. B.; Béguin, F. The Large Electrochemical Capacitance of Microporous Doped Carbon Obtained by Using a Zeolite Template. *Adv. Funct. Mater.* **2007**, *17*, 1828−1836.
(34) Li, Z.; Zhang, L.; Amirkhiz, B. S.; Tan, X.; Xu, Z.; Wang, H.; Olsen, B. C.; Holt, C. M. B.; Mitlin, D. Carbonized Chicken Eggshell Membranes with 3D Architectures as High-Performance Electrode Materials for Supercapacitors. *Adv. Energy Mater.* **2012**, *2*, 431−437.
(35) Ra, E. J.; Raymundo-Piñero, E.; Lee, Y. H.; Béguin, F. High Power Supercapacitors Using Polyacrylonitrile-Based Carbon Nanofiber Paper. *Carbon* **2009**, *47*, 2984−2992.
(36) Li, Q.; Jiang, R.; Dou, Y.; Wu, Z.; Huang, T.; Feng, D.; Yang, J.; Yu, A.; Zhao, D. Synthesis of Mesoporous Carbon Spheres with a Hierarchical Pore Structure for the Electrochemical Double-Layer Capacitor. *Carbon* **2011**, *49*, 1248−1257.
(37) Hao, G.-P.; Lu, A.-H.; Dong, W.; Jin, Z.-Y.; Zhang, X.-Q.; Zhang, J.-T.; Li, W.-C. Sandwich-Type Microporous Carbon Nanosheets for Enhanced Supercapacitor Performance. *Adv. Energy Mater.* **2013**, *3*, 1421−1427.
(38) Gogotsi, Y.; Simon, P. True Performance Metrics in Electrochemical Energy Storage. *Science* **2011**, *334*, 917−918.
(39) Lei, Z.; Lu, L.; Zhao, X. S. The Electrocapacitive Properties of Graphene Oxide Reduced by Urea. *Energy Environ. Sci.* **2012**, *5*, 6391−6399.
(40) Stoller, M. D.; Ruoff, R. S. Best Practice Methods for Determining an Electrode Material's Performance for Ultracapacitors. *Energy Environ. Sci.* **2010**, *3*, 1294−1301.
(41) Yang, L.; Cheng, S.; Ding, Y.; Zhu, X.; Wang, Z. L.; Liu, M. Hierarchical Network Architectures of Carbon Fiber Paper Supported Cobalt Oxide Nanonet for High-Capacity Pseudocapacitors. *Nano Lett.* **2011**, *12*, 321−325.
(42) Biswas, S.; Drzal, L. T. Multilayered Nanoarchitecture of Graphene Nanosheets and Polypyrrole Nanowires for High Performance Supercapacitor Electrodes. *Chem. Mater.* **2010**, *22*, 5667−5671.